

IUE OBSERVATIONS OF HYDROGEN AND DEUTERIUM IN THE LOCAL INTERSTELLAR MEDIUM

J. MURTHY, R. C. HENRY, AND H. W. MOOS
 Department of Physics and Astronomy, Johns Hopkins University

W. B. LANDSMAN
 S.A.S.C. Technologies

J. L. LINSKY¹
 Joint Institute for Laboratory Astrophysics, University of Colorado,
 and National Bureau of Standards

A. VIDAL-MADJAR
 Institut d'Astrophysique de Paris

AND

C. GRY
 Astrophysics Division, Space Science Department, IUE Observatory, ESA, Madrid
 Received 1986 August 4; accepted 1986 October 1

ABSTRACT

We present and analyze high-dispersion IUE observations of the interstellar hydrogen and deuterium Ly α absorption profiles toward the late-type stars ϵ Eri (3.3 pc), Procyon (3.5 pc), Altair (5.1 pc), Capella (13.2 pc), and HR 1099 (33 pc). We confirm the values for $n_{\text{H I}}$, $b_{\text{H I}}$, and $n_{\text{D I}}/n_{\text{H I}}$ derived from previous *Copernicus* data toward ϵ Eri and Procyon but find an average H I density toward HR 1099 of $0.009 \text{ cm}^{-3} \leq n_{\text{H I}} \leq 0.016 \text{ cm}^{-3}$ and a velocity dispersion of $8.8 \text{ km s}^{-1} \leq b_{\text{H I}} \leq 17.7 \text{ km s}^{-1}$ toward Capella, both somewhat larger than those found through *Copernicus* observations. The H I absorption profile toward Altair shows a broad, saturated core and steep line wings, supporting the existence of several velocity components within 5 pc of the Sun. Improved values for the interstellar bulk velocities are generally consistent with a bulk flow from the direction of the galactic center but do show local variations from a uniform flow.

Interstellar deuterium is detected toward every star except Altair, and the derived values for the D/H ratio are consistent with those previously found using *Copernicus* data. In particular, the strong lower limit of $\text{D}/\text{H} \geq 1.9 \times 10^{-5}$ is confirmed for the Capella sightline. A value of $\text{D}/\text{H} = 2.0 \times 10^{-5}$ is consistent with all observations of late-type stars; however, the lower values of D/H found toward several hot stars may indicate real variations in the D/H ratio in the local interstellar medium.

Subject headings: interstellar: abundances — ultraviolet: spectra

I. INTRODUCTION

Studies of the local interstellar medium (Bruhweiler 1984; Cowie and Songaila 1986) indicate that the Sun is located near the edge of a warm, low-density ($n_{\text{H I}} \approx 0.1 \text{ cm}^{-3}$, $T \approx 10^4 \text{ K}$) cloud (analogous to the warm, ionized medium of McKee and Ostriker 1977) which, in turn, is probably embedded in a hot, diffuse ($n_{\text{H I}} \approx 10^{-2}$ – 10^{-3} cm^{-3} , $T \approx 10^6 \text{ K}$) substrate (analogous to the hot, ionized medium of McKee and Ostriker 1977). The bulk of this warm cloud lies toward the galactic center with a total column density of 10^{19} cm^{-2} , dropping to 10^{18} cm^{-2} in most other directions (Bruhweiler 1984). More recent ground-based observations by Lallement, Vidal-Madjar, and Ferlet (1986) indicate that the region of greatest column density (toward the galactic center) may actually be comprised of several velocity components.

Ultraviolet observations of interstellar absorption against either stellar continuum emission, in the case of hot stars, or chromospheric stellar line emission, in the case of cool stars, have provided one of the more fruitful sources of information about the interstellar medium. In particular, the only direct measurements of local (within 50 pc) H I densities ($n_{\text{H I}}$) and

velocity dispersions ($b_{\text{H I}}$) have come through observations of interstellar H I absorption against the chromospheric Ly α emission line of nearby late-type stars. The corresponding interstellar D I absorption feature may be seen at its isotopic blueshift of 80 km s^{-1} relative to the interstellar H Ly α line, and the deuterium-to-hydrogen ratio ($n_{\text{D I}}/n_{\text{H I}}$) may be derived.

In previous papers we have published the results of our observations toward several nearby, late-type stars, both with the *International Ultraviolet Explorer* satellite (IUE) (Landsman *et al.* 1984, 1986) and with the *Copernicus* satellite (Anderson *et al.* 1978, and references therein). Here, we present high-resolution ($\Delta\lambda \approx 0.1 \text{ \AA}$) Ly α spectra of five late-type stars (Table 1), ranging in distance from ϵ Eri (3.3 pc) to HR 1099 (33 pc), taken with the short-wavelength (SWP) camera on IUE. From these spectra we have derived the density ($n_{\text{H I}}$), velocity dispersion ($b_{\text{H I}}$), and bulk velocity ($v_{\text{H I}}$) of the interstellar H I toward each of the stars in Table 1. We have also placed lower limits on the deuterium-to-hydrogen ratio ($n_{\text{D I}}/n_{\text{H I}}$) toward the same stars.

II. OBSERVATIONS AND DATA ANALYSIS

Table 2 summarizes the images analyzed in this paper. These images consist of those taken by us in 1985 together with several archival images obtained through the Regional Data

¹ Staff Member, Quantum Physics Division, National Bureau of Standards.

TABLE 1
STARS OBSERVED

Star	Type	l	b	d (pc)	V_r (km s $^{-1}$)
ϵ Eri	K2 V	196	-48	3.3	+15
α CMi (Procyon)	F5 IV-V	214	13	3.5	-3
α Aql (Altair)	A7 IV-V	48	-9	5.1	-26
α Aur (Capella)	G6 III+G0 III	163	5	13.2	29.1
HR 1099	K0 IV+G0 V	185	-41	33	-14

Analysis Facility (RDAF). The three images of Capella were reprocessed by the National Space Science Data Center (NSSDC) in 1985 to take advantage of the higher resolution available with the new processing software (Bohlin and Turnrose 1982).

The allowable range of our derived parameters is dependent upon the uncertainties inherent in our data. Unfortunately, because *IUE* is not a photon-counting instrument, and for other reasons (Ayres 1982), it is difficult to quantify these errors. We have therefore followed a conservative procedure

TABLE 2
OBSERVING LOG

Image	Date	Exposure Time (minutes)	Aperture ^a	Observer ^b
ϵ Eri				
SWP 26467	1985 Jul 24	540	S ^c	
SWP 26919	1985 Oct 12	435	S ^d	
SWP 27141	1985 Nov 19	375	L ^e	
Procyon				
SWP 20048	1983 May 22	110	L	Ayres
SWP 21194	1983 Sep 30	60	L	Ayres
SWP 21195	1983 Sep 30	60	L	Ayres
SWP 21196	1983 Sep 30	60	L	Ayres
SWP 26917	1985 Oct 11	200	S	
Altair				
SWP 3427	1978 Nov 23	100	L	
SWP 23043	1984 Apr 19	250	L	Giampapa
SWP 26465	1985 Jul 23	240	S ^c	
Capella				
SWP 1454 ^f	1978 May 1 ^g	90	S	Linsky
SWP 2352 ^f	1978 Aug 21 ^g	60	S	Linsky
SWP 8179 ^f	1980 Mar 6 ^h	60	S	Ayres
HR 1099				
SWP 27236	1985 Dec 8 ⁱ	385	S	
β Dra				
SWP 5437	1979 Jun 4	360	L	Stencel/ Linsky/Basri

^a Large aperture closed for all small-aperture observations unless otherwise noted.

^b If no observer is listed, observation was by our group in 1985.

^c Large aperture inadvertently left open.

^d Particle hit at Ly α .

^e Star offset from center of aperture.

^f Reprocessed by NSSDC in 1985.

^g Phase at midpoint of observation is 0.27.

^h Phase at midpoint of observation is 0.75.

ⁱ Phase at midpoint of observation is 0.50.

(Landsman *et al.* 1986) by combining the errors due to camera noise, estimated from a flux-free region near the Ly α line, in quadrature with the photon noise, assuming a 12:1 signal-to-noise ratio (Joseph 1985).

All of the spectra for each star were then placed in the stellar rest frame, normalized, and co-added, with each spectrum weighted proportional to the square of its signal-to-noise ratio. With the exception of the three Procyon images taken during the same shift (SWP 21194, SWP 21195, and SWP 21196), the difference in apparent radial velocity between the different *IUE* spectra for a given star (due primarily to Earth's motion around the Sun) was greater than the pixel spacing of 5.5 km s $^{-1}$ necessary for independent data points, so that the pixel-dependent photometric errors were uncorrelated between different spectra. As fixed pattern noise might contribute to each of the three Procyon images, they were co-added assuming no reduction in camera noise.

Geocoronal and interplanetary Ly α emission imaged through either the small (3" diameter circle) aperture or the large (10" \times 20") aperture must be removed from each spectrum before co-addition. Geocoronal Ly α emission imaged through the small aperture is weak and was easily eliminated by deleting from the spectrum the three data points around its predicted position. When possible, the observations were made at such times that geocoronal Ly α emission fell in the middle of the interstellar absorption core, where it could easily be identified. Geocoronal Ly α emission imaged through the large aperture is a more serious problem, often being close in strength to the stellar emission, and will be dealt with on an individual basis for each star below. (When the background used by IUESIPS was contaminated by spillover from geocoronal Ly α into the interorder pixels, the affected data points were replaced by points from a neighboring wavelength region.)

The data analysis follows the basic procedure of Anderson *et al.* (1978). The stellar emission line, modeled by either a three-parameter Gaussian or a five-parameter solar-type profile (Bruner and Rense 1969), is multiplied by Voigt absorption profiles for interstellar H I and D I, with the neutral hydrogen density (n_{H}), velocity dispersion (b_{H}), and bulk velocity (v_{H}) and the deuterium-to-hydrogen ratio ($n_{\text{D I}}/n_{\text{H}}$) as free parameters. In computing the interstellar absorption profiles we have assumed a uniform, thermally broadened interstellar medium along the line of sight, i.e., we have assumed a single cloud where $b_{\text{D I}} = b_{\text{H}}/2^{1/2}$. The theoretical profile is then convolved with a Gaussian instrumental profile with a FWHM of 0.1 Å (Evans and Imhoff 1985) and a χ^2 goodness-of-fit test is computed. Each of the free parameters used in our procedure is varied until χ^2 is minimized. We note that our procedure uses the center of the stellar Ly α line as a wavelength reference and is thus independent of the nominal *IUE* wavelength scale.

Since we are using a simple model for both the stellar emission profile and the interstellar absorption profile, the quality and applicability of our assumptions should be discussed. Our most critical assumptions are that the stellar profile can be modeled simply by either a Gaussian or a solar-type symmetric profile and that there is a single cloud along the line of sight.

The latter assumption is certainly not valid toward Altair, in which direction Ferlet, Lallement, and Vidal-Madjar (1986) have found at least three distinct velocity components. However, toward the four other stars in Table 1, all in the same quadrant of the sky, the evidence favors a single velocity component. As will be shown later, we find very similar interstellar parameters toward each of these four stars and, in addition, we

find the same H I column densities toward the more distant stars, Capella and HR 1099, as we do toward the nearby stars, ϵ Eri and Procyon. This implies a single cloud extending ~ 3.5 pc in the direction of the four stars with very little H I beyond this cloud, a conclusion supported by the results of Bruhweiler and Kondo (1982), who also find the same column density ($\log N[\text{H I}] = 17.9 \text{ cm}^{-2}$) toward the hot, white dwarf G191-B2B ($d = 48 \text{ pc}$, $l = 156^\circ$, $b = 7^\circ$). Further support for this conclusion comes from the data of Lallement, Vidal-Madjar, and Ferlet (1986), who find only one component toward the star η Aur ($d = 45 \text{ pc}$, $l = 165^\circ$, $b = 0^\circ$), the only star in their sample which is in the same part of the sky as the four stars previously described.

If there is more than one cloud in the line of sight, the derived interstellar parameters may be incorrect; for example, two warm clouds may be blended together to give the appearance of a much hotter cloud. Our assumption of thermal broadening [$b_{\text{D I}} = b_{\text{H I}}/\sqrt{2}$] is not critical in this analysis, since our data are not of sufficient quality to distinguish between thermal and turbulent ($b_{\text{D I}} = b_{\text{H I}}$) broadening, and we have found very little difference in the parameters derived with either assumption.

The interstellar H I column density toward each star is sufficiently large that the Ly α absorption line is saturated over a broad wavelength region, rendering it impossible to observe any structure, such as self-reversal, in the center of the stellar emission line. Thus, the derived interstellar parameters are nearly independent of the assumed stellar profile, provided it is symmetric. Since interstellar absorption itself may cause an asymmetry in the observed line, especially if there is a large difference between the stellar radial velocity and the interstellar wind velocity in that direction, any asymmetry in the intrinsic stellar line may lead to errors in the derived interstellar parameters. This could be of particular importance in the case of spectroscopic binaries where the superposition of the individual stellar spectra at different phases may produce a more complicated, perhaps asymmetric, combined profile. We therefore observed binary stars at conjunction, whenever possible, at which time the combined profile can be expected to be most nearly symmetric.

Evidence that our model does yield realistic values for the interstellar parameters is given by Landsman *et al.* (1986), who have shown that despite their different stellar types, *IUE* observations of α Cen A (G2 V) and α Cen B (K1 V) yield consistent results for the interstellar parameters along that line of sight. Also, as will be shown later, the parameters derived in the present paper are similar to those found toward the same stars through *Copernicus* observations.

Since all of our target stars have also been observed by *Copernicus*, a discussion of the relative merits of *Copernicus* and *IUE* for interstellar studies is appropriate. The higher resolution of *Copernicus* (0.05 Å) compared to *IUE* (0.1 Å) allows a better determination of interstellar D I than is possible with *IUE*. On the other hand, *IUE* results for interstellar H I may be more reliable because of its better background subtraction and because *Copernicus* spectra often did not cover the entire stellar emission line. *IUE* may also be superior in observations of short-period binary stars, such as HR 1099, for which the lower sensitivity of *Copernicus* made it necessary to average over several orbital phases, complicating the data analysis. On the other hand, a single exposure at conjunction was sufficient to acquire a good quality profile of HR 1099 with *IUE*.

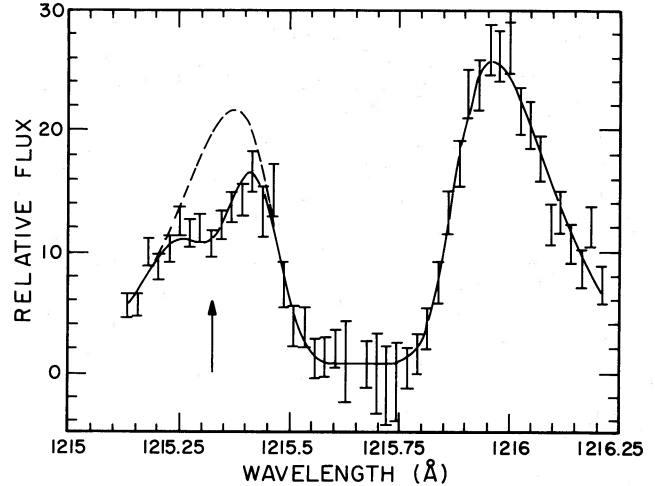


FIG. 1.—The ϵ Eri Ly α profile observed with *IUE* is plotted as $\pm 1 \sigma$ error bars. Solid line is best-fit model profile ($n_{\text{H I}} = 0.12 \text{ cm}^{-3}$, $n_{\text{D I}}/n_{\text{H I}} = 1.4 \times 10^{-3}$, $b_{\text{H I}} = 13.9 \text{ km s}^{-1}$), while dashed line is a model with the same parameters, except that the interstellar D I density has been set to zero. Arrow shows the predicted center of interstellar D I absorption. The stellar emission profile is modeled by a Gaussian with a FWHM of 0.52 Å.

III. RESULTS

a) ϵ Eri

We observed ϵ Eri 3 times (Table 2), but unfortunately each of the extracted Ly α spectra was contaminated either by geocoronal Ly α imaged through the large aperture or by particle hits. The extracted spectra were placed in the stellar rest frame, all contaminated points were given zero weight, and the spectra were co-added. The resultant profile is shown in Figure 1 with the best-fit model to the data superposed.

For this line of sight, as with the others in our survey, interstellar H I absorption lies on the square-root portion of the curve of growth, so that the absorption profile is relatively independent of $b_{\text{H I}}$ resulting in a large range of $n_{\text{H I}}$ and $b_{\text{H I}}$ being compatible with the data. Interstellar D I absorption, on the other hand, is just beginning to enter the flat part of the curve of growth and is thus very sensitive to the velocity dispersion. Unfortunately, because the D I absorption profile lies on the blue wing of the H I absorption line, we cannot parametrize interstellar D I independently of interstellar H I. In order to emphasize the relationship between the D I and H I parameters, and because it is the cosmologically important parameter, we use the deuterium-to-hydrogen ratio ($n_{\text{D I}}/n_{\text{H I}}$), rather than $n_{\text{D I}}$ directly, to model the D I absorption line.

Since the three parameters characterizing the interstellar medium ($n_{\text{H I}}$, $b_{\text{H I}}$, and $n_{\text{D I}}/n_{\text{H I}}$) are closely correlated, standard error bars for each parameter are not meaningful; instead, we use contour plots of one parameter against another, constructed according to the method of Lampton, Margon, and Bowyer (1976). Figures 2a, 2b, and 2c show, respectively, contour plots of $b_{\text{H I}}$ against $n_{\text{H I}}$, $n_{\text{D I}}/n_{\text{H I}}$ against $n_{\text{H I}}$, and $b_{\text{H I}}$ against $n_{\text{D I}}/n_{\text{H I}}$. The meaning of these plots is perhaps best illustrated by discussing a particular example. In Figure 2a, which is a plot of $b_{\text{H I}}$ against $n_{\text{H I}}$, the 90% confidence interval for $b_{\text{H I}}$ with $n_{\text{H I}} = 0.1 \text{ cm}^{-3}$ is $11.4 \leq b_{\text{H I}} \leq 16.1 \text{ km s}^{-1}$, regardless of the values of the other parameters.

The very broad range of acceptable values for each of the three parameters is apparent from Figure 2, but, although we can place no limits on $b_{\text{H I}}$ and no lower limit on $n_{\text{H I}}$, we can set

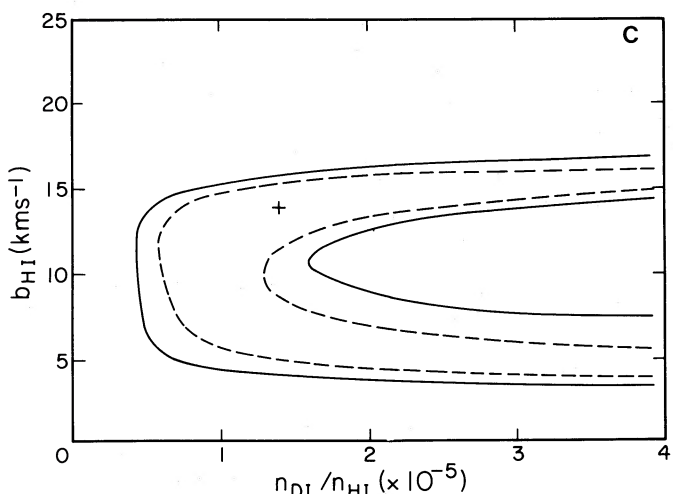
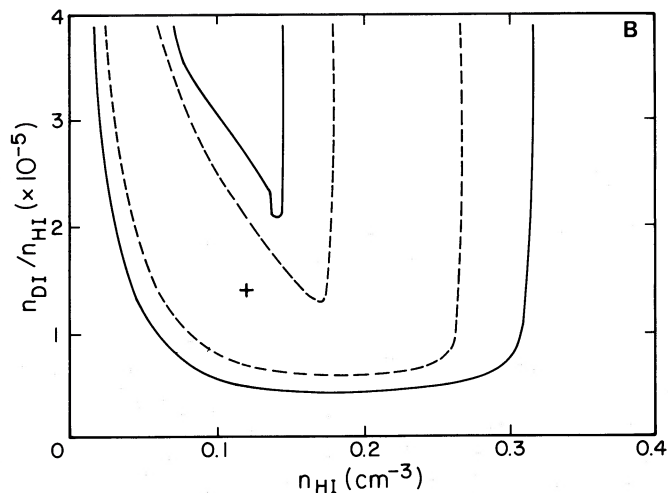
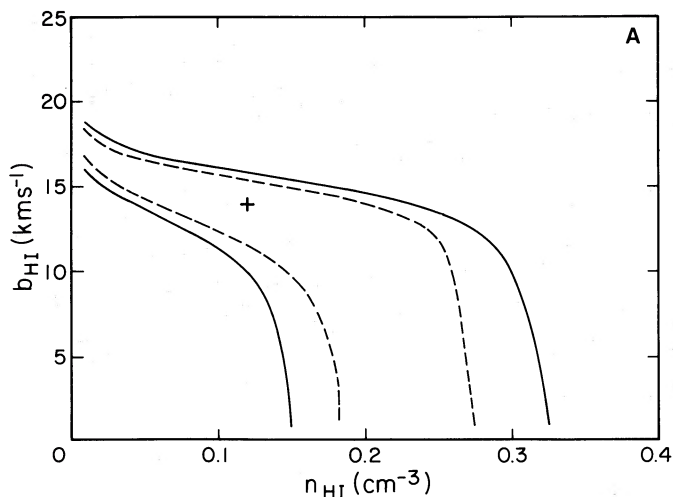


FIG. 2.—Contour plots of (a) b_{HI} , (b) $n_{\text{DI}}/n_{\text{HI}}$ vs. n_{HI} , and (c) b_{HI} vs. $n_{\text{DI}}/n_{\text{HI}}$ are plotted for ϵ Eri. Solid line is a 90% confidence contour, and dashed line is a 50% confidence contour. Contour lines are incomplete at the ends because of the finite grid size, as is also the case for the other contour plots. The position of the best-fit profile of Fig. 1 is plotted as a cross in each of the plots.

an upper limit of 0.32 cm^{-3} for n_{HI} at the 90% confidence level. The effects of interstellar D I absorption are clearly shown by the difference between the dashed line, a model with no interstellar D I, and the best-fit profile (solid line) in Figure 1 and, from Figures 2b and 2c, we can set a lower limit of 4×10^{-6} for $n_{\text{DI}}/n_{\text{HI}}$.

Figure 2a illustrated the insensitivity of the H I profile to the velocity dispersion for n_{HI} greater than $\sim 0.18 \text{ cm}^{-3}$. This, in turn, allows $n_{\text{DI}}/n_{\text{HI}}$ to be virtually unbounded upward for n_{HI} greater than 0.18 cm^{-3} because as n_{DI} increases, the D I absorption feature can still be fitted by decreasing b_{HI} (and thus b_{DI}) without affecting the H I absorption profile. (The sharp rise in $n_{\text{DI}}/n_{\text{HI}}$ at small values of n_{HI} is due simply to the decreasing H I density; i.e., n_{DI} remains constant, while n_{HI} decreases.)

A summary of these results together with a comparison with previous results will be given in a later section.

b) Procyon

Although we were able to observe Procyon only once through the small aperture (SWP 16919), we also analyzed several archival large-aperture images (Table 2). The date of our observation was chosen to place geocoronal Ly α emission in the center of the interstellar absorption core where it was easily identified and the affected points removed from the data. Geocoronal Ly α emission imaged through the large aperture was, however, much harder to separate from the stellar emission, but, unlike the large-aperture ϵ Eri observations, where the geocoronal Ly α emission was comparable to the stellar emission, the peak geocoronal emission in the large-aperture Procyon images was only $\sim 20\%$ of the peak stellar emission. We therefore decided to subtract the geocoronal background and co-add the spectra in order to improve the signal-to-noise ratio.

In subtracting the geocoronal and interplanetary Ly α emission, we used the same procedure as Landsman *et al.* (1984). A sample sky background (SWP 5437) was scaled to the sky background in each of the large-aperture Procyon images and then subtracted from each Procyon image. The sample sky background consisted of an observation of β Dra, which is far enough away (200 pc) that its own Ly α emission is completely absorbed by the interstellar medium. The scaling of the sample background was such that, after subtraction, the resultant flux in the H I absorption core of each Procyon image was zero, as expected for any reasonable interstellar H I density.

A possible problem with this procedure is that the geocoronal and interplanetary components may be separated by as much as 40 km s^{-1} , depending on the time of year and the viewing direction, and may be resolved spectroscopically in large-aperture, high-dispersion IUE images (Clarke *et al.* 1984). The only one of our large-aperture Procyon images where the velocity separation between the geocoronal and interplanetary emissions is significant is image SWP 20048, where the velocity separation is almost 40 km s^{-1} . However, since this observation was through the sunlit geocorona, interplanetary Ly α emission is expected to be negligible compared to the geocoronal emission, implying that the shape of the background feature is the same as image SWP 5437, our sample sky background. (In the other large-aperture Procyon images and in image SWP 5437 the velocity separation is less than 5 km s^{-1} , below the resolution of IUE.)

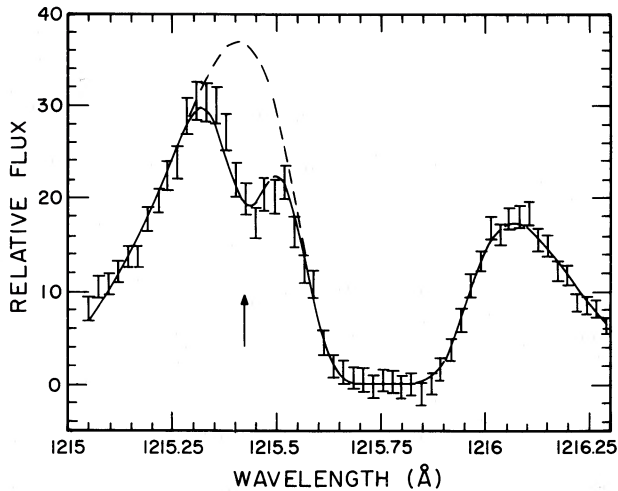


FIG. 3.—Procyon profile is plotted as $\pm 1 \sigma$ error bars. As in Fig. 1, solid line is the best-fit model profile ($n_{\text{HI}} = 0.14 \text{ cm}^{-3}$, $n_{\text{D I}}/n_{\text{HI}} = 1.3 \times 10^{-5}$, $b_{\text{HI}} = 12.2 \text{ km s}^{-1}$), while dashed line is a model with the same parameters except that the interstellar D I density has been set to zero. Arrow shows the predicted center of interstellar D I absorption. The stellar emission profile is modeled by a Gaussian with a FWHM of 0.64 \AA .

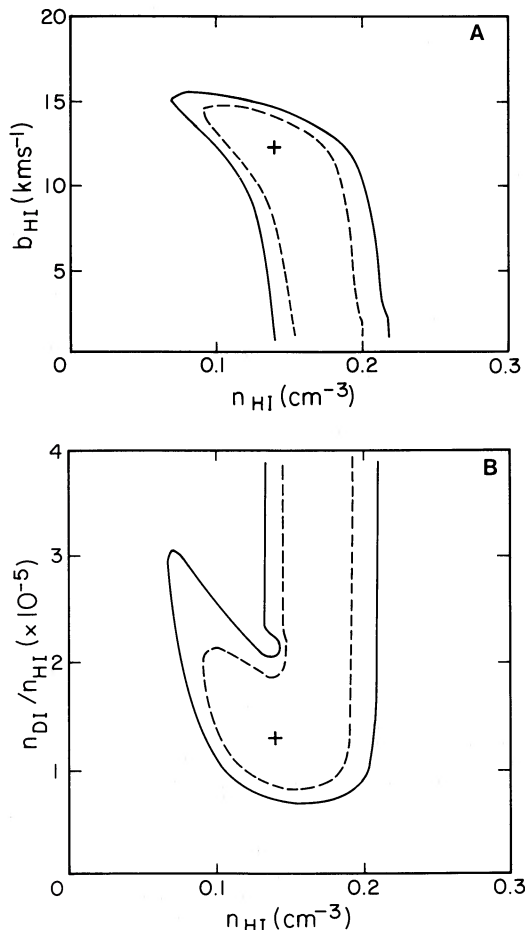


FIG. 4.—Contour plots of (a) b_{HI} vs. n_{HI} , (b) $n_{\text{D I}}/n_{\text{HI}}$ vs. n_{HI} , and (c) b_{HI} vs. $n_{\text{D I}}/n_{\text{HI}}$ are plotted for Procyon. Solid line is a 90% confidence contour, and dashed line is a 50% confidence contour. The position of the best-fit profile in Fig. 3 is plotted as a cross in each of the plots.

TABLE 3
ORBITAL PARAMETERS, BINARY STARS

Parameter	HR 1099 ^a	Capella ^b
P	2.84 days	104.0 days
γ	-14 km s^{-1}	29.1 km s^{-1}
e	0.027	0.0147
T_0	2,442,763.909	2,433,376.765
K_1	50.2 km s^{-1}	26.45 km s^{-1}
K_2	61.6 km s^{-1}	27.47 km s^{-1}
ω	356°	343.04°

^a Bopp and Fekel 1976.

^b Struve and Kilby 1953, with corrections to the zero epoch by Heintz 1975.

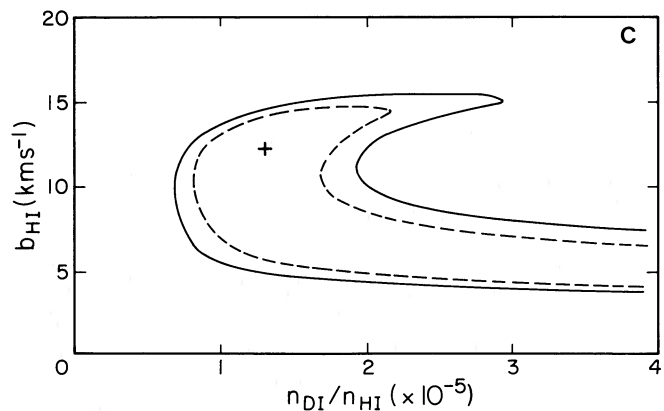
After the geocoronal Ly α emission was subtracted from each image, the large-aperture spectra were co-added. Since the geocoronal subtraction is somewhat uncertain, no reduction in the assumed error bars was made in the geocoronal contaminated region, i.e., the errors in the contaminated region (essentially all but the blue wing) were taken to be the same as those in the best exposed image (SWP 20048). Finally, the sum of the large-aperture spectra was co-added to the small-aperture spectrum.

The final profile is plotted in Figure 3. The region around the D I absorption feature was determined primarily by image SWP 26919, while the wings of the stellar line depend mainly on the large-aperture spectra. Also shown in Figure 3 is the best-fit model profile to the data (solid line).

Much of the discussion about ϵ Eri is also applicable to Procyon, and to the other stars in our program. Figures 4a, 4b, and 4c show, respectively, contour plots of b_{HI} versus n_{HI} , $n_{\text{D I}}/n_{\text{HI}}$, and b_{HI} versus $n_{\text{D I}}/n_{\text{HI}}$. From these plots, we can place 90% limits on n_{HI} ($0.06 \leq n_{\text{HI}} \leq 0.21 \text{ cm}^{-3}$), b_{HI} ($b_{\text{HI}} \leq 16 \text{ km s}^{-1}$), and $n_{\text{D I}}/n_{\text{HI}}$ ($n_{\text{D I}}/n_{\text{HI}} \geq 6 \times 10^{-6}$). The effects of D I absorption can also be seen clearly from the dashed line in Figure 3, a model fitted for no interstellar D I.

c) HR 1099

HR 1099 is a short-period RS CVn binary with orbital parameters summarized in Table 3. The high orbital velocity amplitude ($\sim 50 \text{ km s}^{-1}$) of either component of the binary system complicates the data analysis except when the system is observed at conjunction, when the stellar emission line is likely to be most symmetric. Unfortunately, due to the constraints of IUE scheduling, it was not possible simultaneously to observe



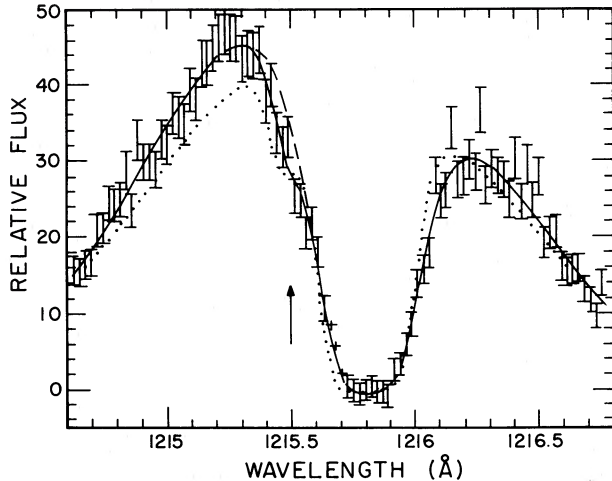


FIG. 5.—The HR 1099 Ly α profile is plotted as $\pm 1 \sigma$ error bars. The three points identified as being contaminated by geocoronal Ly α (see text) are shown as crosses. Solid line is the best-fit model profile ($n_{\text{H I}} = 0.0125 \text{ cm}^{-3}$, $b_{\text{H I}} = 8.3 \text{ km s}^{-1}$, $n_{\text{D I}}/n_{\text{H I}} = 4.3 \times 10^{-6}$), while dashed line is equivalent to the solid line but with the D I density set to zero. Arrow shows the predicted center of interstellar D I absorption. Dotted line is a model profile based on the parameters derived by Anderson and Weiler (1978) ($n_{\text{H I}} = 0.005 \text{ cm}^{-3}$, $b_{\text{H I}} = 14.6 \text{ km s}^{-1}$, $n_{\text{D I}}/n_{\text{H I}} = 1.6 \times 10^{-5}$). The stellar emission line is modeled by a Gaussian with a FWHM of 1.4 Å.

HR 1099 at velocity conjunction and to center geocoronal Ly α in the interstellar H I absorption core. The date of our observation was chosen such that conjunction fell in the middle of our shift, at which time the position of geocoronal Ly α emission (in the stellar rest frame) was calculated to be 1215.675 Å, just at the blue edge of the interstellar absorption core.

Our modeling procedure determined the center of the stellar emission to be at 1215.65 Å, indicating an error of 5 km s $^{-1}$ in the *IUE* wavelength scale. In our final profile of HR 1099 (Fig. 5), the position of geocoronal Ly α is centered at 1215.655 Å, indicated by the arrow, and three points, shown as crosses in Figure 5, were eliminated to account for possible geocoronal contamination. Twelve data points exceeded the highest calibrated levels of the intensity transfer function (ITF), but, since the raw data numbers were all less than 216 DN, these points were given full weight in our procedure.

Figures 6a and 6b show, respectively, contour plots of $b_{\text{H I}}$ versus $n_{\text{H I}}$ and $b_{\text{H I}}$ versus $n_{\text{D I}}/n_{\text{H I}}$. Interstellar D I is detected at a

marginal level, as can be seen from the difference between the dashed line (a model profile with no D I absorption) and the solid line (the best-fit model profile) in Figure 5 and, from the contours in Figure 6b, we place a lower limit at the 90% confidence level of 9×10^{-7} on $n_{\text{D I}}/n_{\text{H I}}$.

From Figure 6 we also place 90% confidence limits of 0.008–0.017 cm $^{-3}$ on $n_{\text{H I}}$ and a 90% confidence upper limit of 15 km s $^{-1}$ on $b_{\text{H I}}$, marginally consistent with the 90% limits of ~ 0.001 –0.008 cm $^{-3}$ and 11–18 km s $^{-1}$ on $n_{\text{H I}}$ and $b_{\text{H I}}$, respectively, set by Anderson and Weiler (1978) through analysis of their *Copernicus* observations of HR 1099. The dotted line plotted in Figure 5 is the best-fit profile determined by Anderson and Weiler ($n_{\text{H I}} = 0.005 \text{ cm}^{-3}$, $b_{\text{H I}} = 14.6 \text{ km s}^{-1}$, $n_{\text{D I}}/n_{\text{H I}} = 1.6 \times 10^{-5}$) degraded to the resolution of *IUE*. This profile is somewhat more symmetrical and has steeper sides on either side of the central dip than we observed with *IUE*. Further *Copernicus* observations of HR 1099 were analyzed by Anderson and Weiler (1979), and they found a higher H I density and a lower velocity dispersion than that derived from the earlier observations. When both *Copernicus* data sets were combined, Anderson and Weiler (1979) found 90% confidence limits of 0.006–0.012 cm $^{-3}$ for $n_{\text{H I}}$ and 10–14 km s $^{-1}$ for $b_{\text{H I}}$, much closer to the values we find from our analysis of the *IUE* data. As previously mentioned, the *Copernicus* profile of HR 1099 consists of observations over several days and is thus an average over the entire orbital period of the binary. Since HR 1099 is highly variable, and because of the asymmetries that may be introduced in this averaging over several different orbital phases and times, the *IUE* results, which were derived from a single observation taken at conjunction, may be more reliable.

d) Capella

Capella is a spectroscopic binary with a period of ~ 104 days (see Table 3 for the orbital parameters) and, like HR 1099, is best observed at velocity conjunction to simplify the modeling of the intrinsic stellar emission line. Since we were unable to observe Capella in our program, we instead analyzed three archival small-aperture images (Table 2) of Capella, which were reprocessed by the NSSDC to take advantage of the higher resolution available with the new image processing software. These images have been discussed from a stellar point of view by Ayres and Linsky (1980) and Ayres, Schiffer, and Linsky (1983).

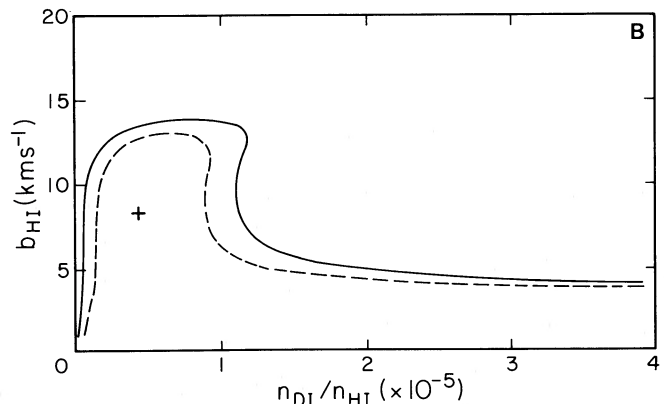
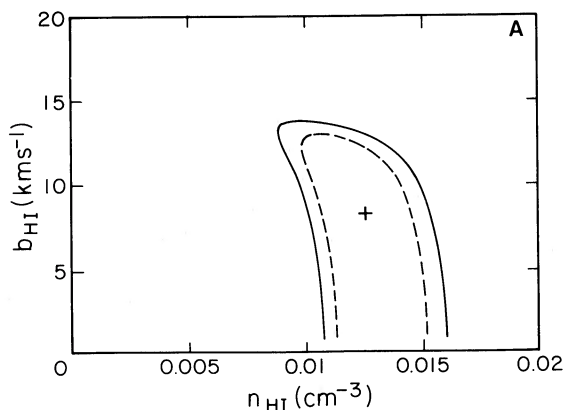


FIG. 6.—Contour plots of (a) $b_{\text{H I}}$ vs. $n_{\text{H I}}$ and (b) $b_{\text{H I}}$ vs. $n_{\text{D I}}/n_{\text{H I}}$ are plotted for HR 1099. Solid line represents a 90% confidence contour, while dashed line represents a 50% confidence contour. Cross marks the position of the best-fit profile in Fig. 5.

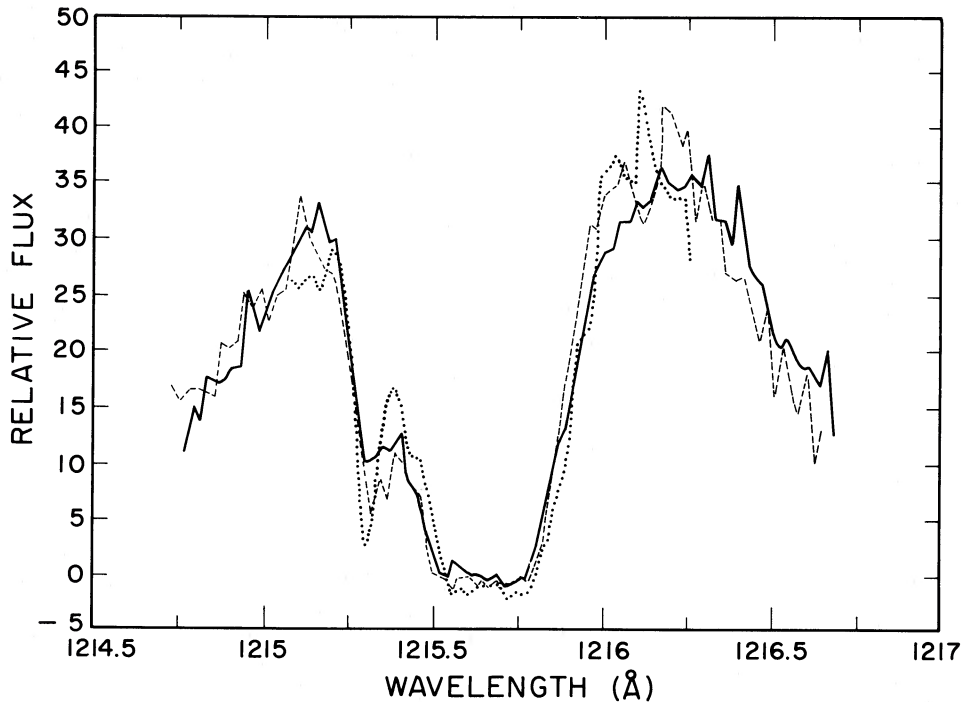


FIG. 7.—Three line profiles of the Ly α emission from Capella are plotted: Profile 1 (solid line), Profile 2 (dashed line), and the Copernicus profile of McClintock *et al.* (1978) (dotted line). Note that the Copernicus profile does not extend over the wings of the stellar line, but the D I feature is more pronounced, because of the higher spectral resolution of Copernicus.

Although geocoronal emission was expected to be minimal, due to the short exposure times, the points surrounding its predicted position were removed from the spectra in images SWP 1454 and SWP 8179. Coincidentally, the observation data for SWP 2352 was such that geocoronal Ly α emission was imaged onto the center of the H I core, but since no emission was seen at its predicted position, no points were removed from the data. Two of the images (SWP 1454 and SWP 2352) were obtained at nearly the same phase (0.25) and were co-added (profile 1), while the other image (SWP 8179) was obtained near phase 0.75 (profile 2).

Plotted in Figure 7 are both profile 1 and profile 2 (solid and dashed lines, respectively) and the Copernicus profile (dotted line) derived by McClintock *et al.* (1978), which is the sum of two observations made by Dupree, Baliunas, and Shipman (1977) at different orbital phases of the binary (phases of ~ 0.25 and 0.5, respectively). All three profiles are similar, implying that there must be a significant contribution to the combined Ly α profile from both components of the binary system, as concluded by Ayres and Linsky (1980). Thus, as the stellar emission profiles appear to be fairly independent of the phase, the derived interstellar parameters should also be independent of the phase as indeed they are, for the most part (see below). This does not appear to be true in the case of HR 1099.

We have analyzed both profile 1 and profile 2, and we have derived similar values for the interstellar parameters using either profile, with the exception of the velocity dispersion. Although consistent at the 90% confidence level, at the 50% confidence level we derive a much higher lower limit for b_{HI} from profile 2 ($14.2 \leq b_{\text{HI}} \leq 19.6 \text{ km s}^{-1}$) than from profile 1 ($8.8 \leq b_{\text{HI}} \leq 17.7 \text{ km s}^{-1}$). Our models do not fit profile 2 very well, especially in the region of the red peak, which is larger with respect to the blue peak than is the case for profile 1 (Fig. 7), and we find a much higher reduced χ^2 for the best-fit model

to profile 2 ($\chi^2 = 1.78$) than for the best-fit model to profile 1 ($\chi^2 = 1.05$). For this reason, and because the signal-to-noise ratio is lower for profile 2 than for profile 1, the results derived from profile 1 are probably more reliable. Figure 8 shows profile 1, with the best-fit model superposed. The stellar emission line was found to be centered $\sim 12 \text{ km s}^{-1}$ from the center of mass velocity in the same direction as the secondary star, unlike profile 2 which was centered at the center of mass velocity. Figures 9a, 9b, and 9c show, respectively, contour plots of

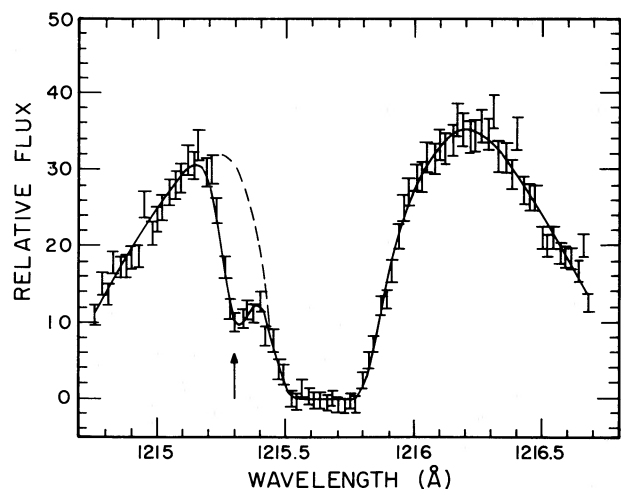


FIG. 8.—Profile 1 (Capella at a phase of 0.25) is plotted as 1σ error bars with the best-fit model profile ($n_{\text{HI}} = 0.015 \text{ cm}^{-3}$, $b_{\text{HI}} = 15.9 \text{ km s}^{-1}$, $n_{\text{D I}}/n_{\text{HI}} = 6 \times 10^{-5}$) superposed (solid line). Dashed line is the same as solid line, except that the D I density has been set to zero. Arrow shows the predicted center of interstellar D I absorption. The stellar emission line is modeled by a solar-type profile with a FWHM of 1.7 \AA .

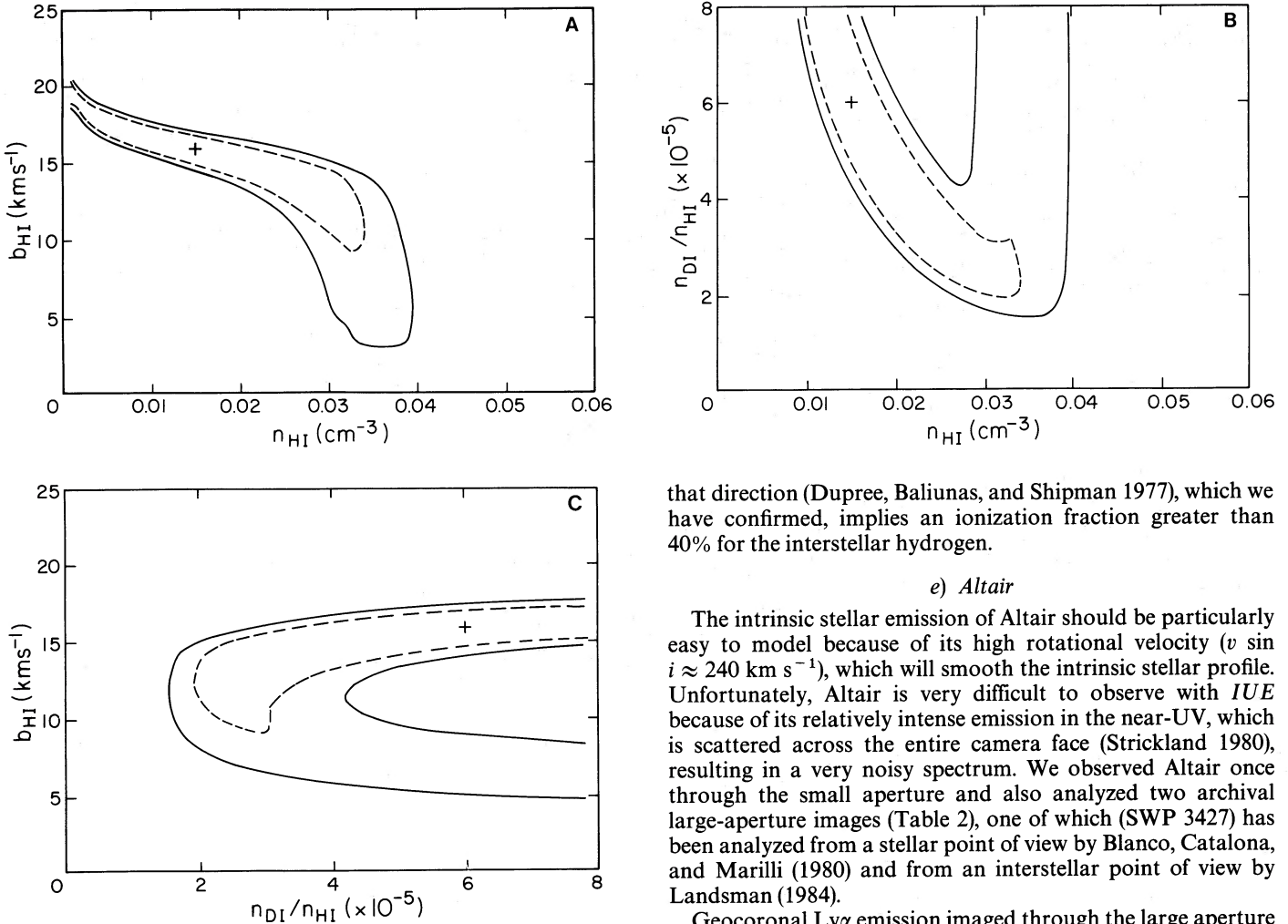


FIG. 9.—Contour plots of (a) b_{HI} vs. n_{HI} , (b) $n_{\text{D I}}/n_{\text{HI}}$ vs. n_{HI} , and (c) b_{HI} vs. $n_{\text{D I}}/n_{\text{HI}}$ for Capella. Solid line is a 90% contour, while dashed line is a 50% contour. Cross shows the position of the best-fit profile plotted in Fig. 8.

b_{HI} against n_{HI} , $n_{\text{D I}}/n_{\text{HI}}$ against n_{HI} , and b_{HI} against $n_{\text{D I}}/n_{\text{HI}}$ derived from profile 1.

McClintock *et al.* (1978) obtained values of $0.04\text{--}0.05\text{ cm}^{-3}$ for n_{HI} , $5\text{--}12\text{ km s}^{-1}$ for b_{HI} , and $1.8 \times 10^{-5}\text{--}4.0 \times 10^{-5}$ for $n_{\text{D I}}/n_{\text{HI}}$ from *Copernicus* observations of Capella. These data were subsequently reanalyzed by Anderson (1979), using a more sophisticated procedure, which yielded 90% confidence limits of $0.02 \leq n_{\text{HI}} \leq 0.04\text{ cm}^{-3}$, $b_{\text{HI}} \leq 15\text{ km s}^{-1}$, and $n_{\text{D I}}/n_{\text{HI}} \geq 2 \times 10^{-5}$, which are entirely consistent with our *IUE* results. At the 50% confidence level, however, we find a somewhat higher range of velocity dispersions ($8.8 \leq b_{\text{HI}} \leq 17.7\text{ km s}^{-1}$) than did Anderson ($3\text{--}12\text{ km s}^{-1}$). It is difficult to determine which results are more reliable as the *Copernicus* data have a much higher signal-to-noise ratio, with a peak of 30:1, than the *IUE* data, which have a peak signal-to-noise ratio of 17:1, while, on the other hand, the *IUE* data cover the entire stellar line, including the wings, which allows a better determination of the intrinsic stellar profile.

Although we cannot directly determine the degree of ionization in the interstellar medium, Bobroff, Nousek, and Garmire (1984) concluded that their failure to observe He II (304 Å) radiation from Capella combined with the low H I density in

that direction (Dupree, Baliunas, and Shipman 1977), which we have confirmed, implies an ionization fraction greater than 40% for the interstellar hydrogen.

e) Altair

The intrinsic stellar emission of Altair should be particularly easy to model because of its high rotational velocity ($v \sin i \approx 240\text{ km s}^{-1}$), which will smooth the intrinsic stellar profile. Unfortunately, Altair is very difficult to observe with *IUE* because of its relatively intense emission in the near-UV, which is scattered across the entire camera face (Strickland 1980), resulting in a very noisy spectrum. We observed Altair once through the small aperture and also analyzed two archival large-aperture images (Table 2), one of which (SWP 3427) has been analyzed from a stellar point of view by Blanco, Catalana, and Marilli (1980) and from an interstellar point of view by Landsman (1984).

Geocoronal Ly α emission imaged through the large aperture contaminates the interstellar absorption core and much of the red peak in both of the large-aperture spectra and also contaminates much of the blue peak in SWP 26465, since the large aperture was inadvertently left open through this observation. In addition, there is a very prominent peak in the middle of the interstellar absorption core, at the predicted position of geocoronal Ly α emission imaged through the small aperture. Although this feature is much larger and more extended than would be expected from the strength of the geocoronal emission observed in our other small-aperture spectra, it was treated as geocoronal emission and was given zero weight, as were all the other geocoronal contaminated points. The three spectra were then placed in the stellar rest frame and co-added. The resultant spectrum is shown in Figure 10 with selected error bars.

Unfortunately the error bars in our data are so large that no formal limits can be set on the derived parameters. Instead we have constructed model profiles for different values of the interstellar parameters and visually determined which are compatible with the data.

Since the presence of D I has very little effect on the model profile for reasonable values of $n_{\text{D I}}/n_{\text{HI}} (\leq 10^{-3})$, we have fixed it at 10^{-5} , an order of magnitude estimate, in all the models discussed below. The best-fit model, plotted as a solid line in Figure 10, is characterized by a very high velocity dispersion ($b_{\text{HI}} = 22.5\text{ km s}^{-1}$) and a high H I density ($n_{\text{HI}} = 0.21\text{ cm}^{-3}$).

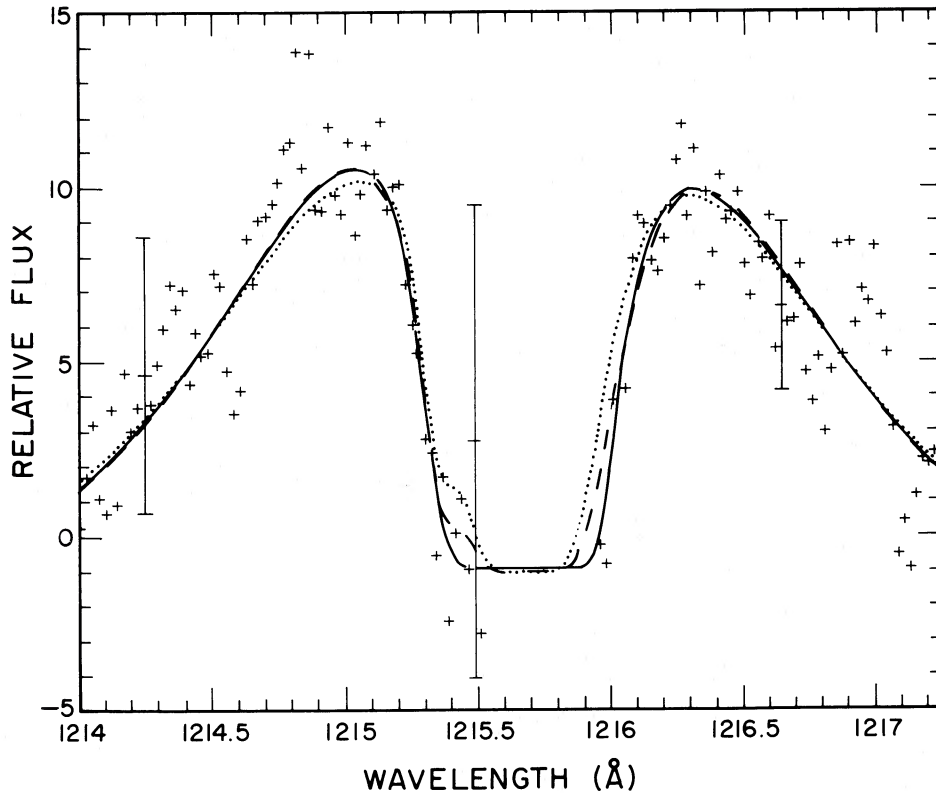


FIG. 10.—Altair data are plotted as crosses with selected representative error bars. There is a lack of data in the core because of geocoronal contamination in each of the spectra. Also plotted are three different model profiles, with $n_{\text{D I}}/n_{\text{H I}}$ fixed at 1.0×10^{-5} : the best-fit profile with $b_{\text{H I}} = 22.5 \text{ km s}^{-1}$ and $n_{\text{H I}} = 0.21 \text{ cm}^{-3}$ (solid line); a model with $b_{\text{H I}} = 13 \text{ km s}^{-1}$ and $n_{\text{H I}} = 0.21 \text{ cm}^{-3}$ (dashed line); and a model with $b_{\text{H I}} = 13 \text{ km s}^{-1}$ and $n_{\text{H I}} = 0.15 \text{ cm}^{-3}$ (dotted line). The stellar emission line is modeled by a Gaussian with a FWHM of 1.9 \AA .

The dashed line in Figure 10 represents a model with a more typical value of $b_{\text{H I}}$ ($b_{\text{H I}} = 13 \text{ km s}^{-1}$) but still with a high value of $n_{\text{H I}}$ ($n_{\text{H I}} = 0.21 \text{ cm}^{-3}$). Although the latter profile appears to fit the data somewhat less well than the best-fit model, there is virtually no difference in the value of χ^2 between the two profiles. This is because the main disagreement between the two profiles is in the fitting of the two points in the red corner of the absorption core where the error bars are very large. De Boer *et al.* (1986) have derived a value of 0.5 cm^{-3} for $n(\text{H})$ toward Altair from their observations of interstellar metal abundance with the balloon-borne ultraviolet spectrophotometer (BUSS), and, if we assume an ionization fraction of 0.7 (e.g., Bertaux 1984), this leads to a value of 0.15 cm^{-3} for $n_{\text{H I}}$ ($N[\text{H I}] = 2.3 \times 10^{18} \text{ cm}^{-2}$). The best-fit model for this density is also fitted with a very high velocity dispersion ($b_{\text{H I}} = 23.5 \text{ km s}^{-1}$) and is virtually indistinguishable from the solid line in Figure 10. The dotted line in Figure 10 shows a model with $n_{\text{H I}} = 0.15 \text{ cm}^{-3}$ and $b_{\text{H I}} = 13 \text{ km s}^{-1}$. Although the χ^2 for this model is not significantly different from the best-fit model, it does not appear to adequately fit the broad absorption core. Models with lower H I densities and similar velocity dispersions are yet narrower and need larger values of $b_{\text{H I}}$ to fit the data.

Thus, from the profiles in Figure 10 and from other trial profiles, it appears that a model with either a high-velocity dispersion or a high H I density (or both) is needed to fit the broad absorption core well; for instance, if we fix $b_{\text{H I}}$ at 13 km s^{-1} , $n_{\text{H I}}$ should be greater than $\sim 0.2 \text{ cm}^{-3}$, while if we fix $n_{\text{H I}}$ at 0.1 cm^{-3} , $b_{\text{H I}}$ should be greater than $\sim 20 \text{ km s}^{-1}$. An

explanation for these atypical interstellar parameters is found from the work of Ferlet, Lallement, and Vidal-Madjar (1986), who have found at least three interstellar components toward Altair, with heliocentric velocities of -17.4 , -21.4 , and -26 km s^{-1} , respectively, through observations of Ca II and Na I absorption lines. These three components could be blended together to form a broad Ly α absorption profile, because of the large optical depth of the ISM at Ly α , which would then lead to an overestimate of the H I density and the velocity dispersion.

f) Bulk Velocities

Bulk velocities for the interstellar gas can be determined fairly accurately by our analysis procedure because of the square-well shape of the interstellar H I absorption profile and because the bulk velocity is determined with respect to the stellar emission line, rather than the IUE wavelength scale. Unfortunately, the combination of the high interstellar H I densities and the low resolution of IUE make it impossible to distinguish between different velocity components in the interstellar medium through IUE Ly α measurements.

There were two cases when the stellar emission line was not centered at the apparent center of mass velocity, both of which have been described above. The stellar Ly α line was centered at 1215.65 \AA for our HR 1099 IUE profile, but, since velocity conjunction fell in the middle of our observation, it was assumed that the stellar emission line was centered at the center of mass velocity for the binary, and that the IUE wavelength scale was incorrect. The other case was profile 1 for

TABLE 4
BULK VELOCITIES

Star (1)	l (2)	b (3)	d (pc) (4)	V_r (km s ⁻¹) (5)	V_{H1} (km s ⁻¹) (6)	V_{LSR} (km s ⁻¹) (7)	V_{WM} (km s ⁻¹) (8)	V_B (km s ⁻¹) (9)	V_C (km s ⁻¹) (10)
ϵ Eri	196	-48	3.3	+15	7.3-15.4 17.9 \pm 7.5 ^a	13.5	20.8	16.5	21.8
Procyon	214	13	3.5	-3	20.8-27.2 17 \pm 7.5 ^b	13.1	18.2	15.1	25.4
Capella	163	5	13.2	+29.1	7.8-28.4 ^c 5.4-27.6 ^d 24.1 \pm 7.5 ^a	4.4	21.5	17.5	20.
HR 1099	185	-41	33	-14	20.4-30.4 23 \pm 7 ^e	12.3	22.7	18.0	22.7
α Cen A	316	-1	1.3	-24.7	-14.7 \pm 3 ^f	2.6	-16	-12.8	-9.8
α Cen B	316	-1	1.3	-19.1	-15.5 \pm 1.9 ^f	2.6	-16	-12.8	-9.8

NOTES.—Col. (6) contains the heliocentric velocities derived toward each star. Except where noted, 50% confidence levels are given. The other columns contain the projections of the velocity of gas moving with the LSR (col. [7]); the velocity found through He I (584 Å) photometry by Weller and Meier 1981 (col. [8]); the velocity found through Ly α photometry by Bertaux 1984 (col. [9]); and the velocity found through optical observations of nearby stars by Crutcher 1982 (col. [10]).

^a McClintock *et al.* 1978; no formal confidence levels given.

^b Anderson *et al.* 1978.

^c This work, phase 0.27.

^d This work, phase 0.75.

^e Anderson and Weiler 1978.

^f Landsman *et al.* 1986; 90% confidence levels.

Capella where the stellar emission line was redshifted by 12 km s⁻¹ from the center of mass velocity. Since the observation was made at quadrature, the stellar Ly α line is not necessarily symmetric about the center of mass velocity, and it was therefore assumed that the *IUE* wavelength scale was correct and the bulk velocities were calculated with respect to the *IUE* wavelength scale. The *IUE* wavelength scale itself is uncertain by up to 6 km s⁻¹ (Turnrose *et al.* 1984), and this possible error has been taken into account in the velocities derived from the Capella spectra. The bulk velocities derived from the analysis of our *IUE* results are summarized in Table 4 and are compared with the our previous *Copernicus* results. The results in Table 4 will be discussed more fully in the next section.

IV. SUMMARY AND DISCUSSION

A summary of our *IUE* results is given in Table 5, together with several previous *Copernicus* results toward the same stars. Our *IUE* results are generally consistent with those previously derived from the analysis of *Copernicus* data, except that we derive a somewhat higher velocity dispersion at the 50% confidence level than did Anderson (1979) for the line of sight to Capella. Since it is not clear whether the *Copernicus* results are more or less reliable than the *IUE* results, the velocity dispersions toward Capella should be treated with care at the 50% confidence level. The high-velocity dispersion found from profile 2 (phase 0.75) should not be considered as reliable as

TABLE 5
SUMMARY OF RESULTS

Star	l	b	d (pc)	n_{H1} (cm ⁻³)	b_{H1} (km s ⁻¹)	$N(H\ I)$ ($\times 10^{17}$ cm ⁻²)	n_{D1}/n_{H1} ($\times 10^{-5}$)	$N(D\ I)$ ($\times 10^{12}$ cm ⁻²)	References
ϵ Eri	196	-48	3.3	0.01-0.27*	3.3-16.6*	2.4-28*	≥ 0.6	≥ 8.1	
Procyon	214	13	3.5	0.06-0.20 0.09-0.2*	4-18 3.4-14.8*	6.1-20 9.7-22*	1.1-2.9 ≥ 0.8	≥ 18.3 ≥ 11.9	1
Altair	48	-9	5.1	0.09-0.13	9-14	9.7-14	0.7-1.9	...	2
Capella	163	5	13.2	3
				0.008-0.033*	8.8-17.7*	6.5-14*	≥ 1.9	≥ 36.2	4
				0.007-0.036*	14.2-19.6*	6.5-13*	≥ 1.8	≥ 26.0	5
				0.022-0.04	3-12	9.5-17	≥ 2.0	...	6
				0.02-0.04	10	9-15	2.2-9.6	...	7
HR 1099	185	-41	33	0.009-0.016*	$\leq 13.1^*$	9.1-16*	≥ 0.09	≥ 1.1	
				0.002-0.007	14-16	2-7.1	1-4.7	...	8
				0.007-0.011	10.5-14	7.1-11.2	0.6-2.5	...	9
α Cen A	316	-1	1.3	0.03-0.21	≥ 11	1.2-8.4	≥ 0.8	...	10
α Cen B	316	-1	1.3	≤ 0.15	≥ 14.3	≤ 6.0	≥ 1.5	...	11

NOTES.—Except where otherwise noted, 50% confidence intervals are given. Asterisk denotes values taken with n_{D1}/n_{H1} forced to lie below 10^{-4} . (The contour plots have no such restriction.)

REFERENCES.—(1) McClintock *et al.* 1978; no formal confidence levels given. (2) Anderson *et al.* 1978. (3) See text. (4) This work, phase 0.27 (profile 1). (5) This work, phase 0.75 (profile 2). (6) Anderson 1979. (7) Dupree, Baliunas, and Shipman 1977; no formal confidence levels given. (8) Anderson and Weiler 1978. (9) Anderson and Weiler 1979. (10) Landsman *et al.* 1984. (11) Landsman *et al.* 1986.

either the velocity dispersion derived from profile 1 (phase 0.25) or that derived from the *Copernicus* observations for the reasons discussed previously. We also obtain a higher interstellar H I density and a lower velocity dispersion toward HR 1099 than did Anderson and Weiler (1978), but further *Copernicus* observations (Anderson and Weiler 1979) removed much of this discrepancy. The *IUE* data may be superior because they were taken at conjunction when the stellar profile can be expected to be most symmetric, while the *Copernicus* data included observations made at several different phases, which may complicate modeling of the stellar profile.

The H I densities and velocity dispersions toward the different stars in Table 5 are consistent with a single cloud with $n_{\text{HI}} \approx 0.1 \text{ cm}^{-3}$, except along the line of sight to Altair. The H I column densities toward Capella and HR 1099 are both on the order of 10^{18} cm^{-2} , the same as those toward the closer stars, ϵ Eri and Procyon, implying that this local cloud does not extend much farther than ~ 3.5 pc in the direction of the four stars. The line of sight to Altair, on the other side of the Sun, is rather more complicated, with at least three different components present (Ferlet, Lallement, and Vidal-Madjar 1986). From the above results, combined with those of Lallement, Vidal-Madjar, and Ferlet (1986), we can draw a picture of the local interstellar medium where the region of greatest column density (toward the galactic center) consists of several components, which may be present even on a scale of 5 pc, while in the opposite direction there may be a single cloud with a total column density of 10^{18} cm^{-2} and a spatial extent of ~ 3.5 pc.

The velocity dispersions appear to lie between ~ 5 and 16 km s^{-1} , corresponding to temperatures between $\sim 1.5 \times 10^3$ and $1.5 \times 10^4 \text{ K}$ (assuming purely thermal broadening), with an average value of $11\text{--}13 \text{ km s}^{-1}$. In general, the velocity dispersions are consistent with a value of $\sim 13 \text{ km s}^{-1}$ nearly everywhere. Again, the line of sight to Altair is an exception, with a minimum b_{HI} of $\sim 20 \text{ km s}^{-1}$ (when $n_{\text{HI}} = 0.1 \text{ cm}^{-3}$). However, if we indeed have more than one component toward Altair, the true velocity dispersions of the individual components may be much less than the apparent velocity dispersion.

These temperatures are in general agreement with those derived through observations of reflected solar radiation from interstellar atoms entering the solar system. Through He I (584 Å) photometry, Weller and Meier (1981) have derived a temperature of $9000\text{--}15,000 \text{ K}$, while Daladier *et al.* (1984), also through He I photometry, found a temperature of $16,000 \pm 5000 \text{ K}$, and Bertaux (1984) derived a temperature of $8000 \pm 1000 \text{ K}$ through Ly α absorption cell photometry. The higher temperatures derived from He I photometry may be caused by interactions with the solar wind (Fahr, Nass, and Rucinski 1985).

Another product of the observations of the interstellar flow into the solar system is that the direction and velocity of the incoming flow can be derived. Weller and Meier (1981) found that the interstellar wind was coming from a direction of $(l, b) = (2^\circ, 16^\circ)$ with a velocity of $22\text{--}28 \text{ km s}^{-1}$, while Bertaux (1984) determined almost the same incoming direction $(l, b) = (4^\circ, 16^\circ)$, but a slightly different velocity of $20 \pm 1 \text{ km s}^{-1}$. As mentioned above, Lallement, Vidal-Madjar, and Ferlet (1986) have found several velocity components in the local interstellar medium. Their observations essentially duplicate those of Crutcher (1982), but at higher resolution and more detail, and for our purpose, the bulk velocity derived by Crutcher, an average of all the components found by Lallement,

Vidal-Madjar, and Ferlet, is more appropriate. This flow is slightly different from those found by Weller and Meier (1981) and Bertaux (1984) for the immediate neighborhood of the Sun, with a velocity of 28 km s^{-1} coming from $(l, b) = (28^\circ, 10^\circ)$. The projections of each of these velocities toward the different stars have been tabulated in Table 4.

Although our sample size is too limited to draw many conclusions, it is apparent that our derived bulk velocities (Table 4) are roughly consistent with an average interstellar bulk flow coming from the general direction of the galactic center, as suggested by Vidal-Madjar *et al.* (1978). There are, however, surprising variations in the bulk velocities along the different lines of sight; for instance, the allowed ranges for the velocities toward ϵ Eri and HR 1099 do not overlap even though the two stars are separated by less than 11° in the sky.

There is some evidence for substantial variations in the D/H ratio in the local interstellar medium (Vidal-Madjar and Gry 1984). Unfortunately, although we do detect D I toward each of our target stars (except Altair), the resolution of *IUE* is too low for us to do more than set lower limits on $n_{\text{D I}}/n_{\text{H I}}$. The most interesting of these lower limits is the 1.9×10^{-5} found along the line of sight to Capella, confirming the results of Dupree, Baliunas, and Shipman (1977) and those of McClintock *et al.* (1978). Vidal-Madjar *et al.* (1986) suggest that an interstellar cloud with a D/H ratio of less than 10^{-5} exists within 15 pc of the Sun and from this and the high D/H value found toward Capella concluded that the D/H ratio varied by at least a factor of 2 over a region of 15 pc or less. There is also some evidence for significant variations in the D/H ratio from our own data (as pointed out by an anonymous referee). If we force b_{HI} to lie above 10 km s^{-1} (6000 K), we can set an upper limit of 1.1×10^{-5} , at the 90% confidence level, on $n_{\text{D I}}/n_{\text{H I}}$ toward HR 1099 (Fig. 6b), much lower than the lower limit of 1.9×10^{-5} found toward Capella. It should be noted that we cannot set a formal upper limit on the D/H ratio toward HR 1099 unless we also set a lower limit on b_{HI} . D I is not observed toward Altair, partly due to the very high noise level and partly due to the very broad absorption profile, which masks any D I absorption.

V. CONCLUSIONS

We have shown that the interstellar medium along the lines of sight to several nearby stars is consistent with a local cloudlet of $n_{\text{HI}} \approx 0.1 \text{ cm}^{-3}$ and $T \approx 10^4 \text{ K}$. The low column densities [$N(\text{H I}) \approx 10^{18} \text{ cm}^{-2}$] toward Capella and HR 1099 indicate that this cloud extends no further than ~ 3.5 pc in that direction. The bulk velocities along the different lines of sight are consistent with an interstellar wind coming from the general direction of the galactic center, perhaps as a result of supernova shocks from the Sco-Oph association (Crutcher 1982), and are clearly not due to the motion of the Sun in the LSR.

Our results generally confirm those of previous *Copernicus* observations toward the same stars, despite the separation of several years between the two sets of observations. Since the chromospheric Ly α emission may vary greatly over this time scale (as does the solar chromospheric emission), this similarity implies that our derived parameters are relatively independent of the intrinsic stellar profile, confirming the conclusions of Landsman *et al.* (1986) from their observations of the α Cen binary system. However, we derive somewhat different parameters from our observations of the binary stars Capella and HR 1099 than from previous *Copernicus* observations, although

these parameters are entirely consistent at the 90% level. Further observations are needed to determine better the relationship between the phase of the binary system and the derived interstellar parameters.

Although our own results are compatible with a uniform D/H ratio everywhere greater than 2×10^{-5} , the results of Vidal-Madjar *et al.* (1986), and our confirmation of the lower limit of 1.8×10^{-5} toward Capella, support the idea of significant variations in the D/H ratio over relatively small scales (<20 pc).

Finally, the line of sight to Altair appears to be qualitatively different from the others, with a very broad H I absorption core, which is fitted by a very high velocity dispersion ($b_{\text{HI}} \approx 22.5 \text{ km s}^{-1}$) or by high H I densities ($n_{\text{HI}} \approx 0.2 \text{ cm}^{-2}$), indicating a multicomponent interstellar medium in that direction, as

found by Ferlet, Lallement, and Vidal-Madjar (1986).

We intend to continue our observations with *IUE* in the current year. Further work on this subject should also be done using the High Resolution Spectrometer (HRS) aboard the Hubble Space Telescope (HST) whose high sensitivity and resolution ($\Delta\lambda \approx 0.01 \text{ \AA}$) should prove ideal for probing interstellar H I and D I.

We thank Dr. Y. Kondo and the staff of the *IUE* observatory for their help in the acquisition and reduction of these data. We also thank the National Space Science Data Center for providing and reprocessing archival *IUE* data.

This work was supported by NASA grant NSG 5393 to the Johns Hopkins University.

REFERENCES

- Anderson, R. C. 1979, Ph.D. thesis, Johns Hopkins University.
 Anderson, R. C., Henry, R. C., Moos, H. W., and Linsky, J. J. 1978, *Ap. J.*, **226**, 883.
 Anderson, R. C., and Weiler, E. J. 1978, *Ap. J.*, **224**, 143.
 ———, 1979, *Pub. A.S.P.*, **91**, 431.
 Ayres, T. R. 1982, *Ap. J.*, **257**, 243.
 Ayres, T. R., and Linsky, J. L. 1980, *Ap. J.*, **241**, 279.
 Ayres, T. R., Schiffer, F. H., and Linsky, J. L. 1983, *Ap. J.*, **272**, 223.
 Bertaux, J. 1984, in *Local Interstellar Medium*, ed. Y. Kondo, F. C. Bruhweiler, and B. D. Savage (NASA CP 2345), p. 3.
 Blanco, C., Catalano, S., and Marilli, E. 1980, in *Proc. 2d European IUE Conference* (ESA SP-157), p. 63.
 Bobroff, N., Housek, J., and Garmire, G. 1984, *Ap. J.*, **277**, 678.
 Bohlin, R. C., and Turnrose, B. E. 1982, *NASA IUE Newsletter*, No. 18, p. 29.
 Bopp, B. W., and Fekel, F. 1976, *A.J.*, **81**, 771.
 Bruhweiler, F. C. 1984, in *Local Interstellar Medium*, ed. Y. Kondo, F. C. Bruhweiler, and B. D. Savage (NASA CP 2345), p. 39.
 Bruhweiler, F. C., and Kondo, Y. 1982, *Ap. J.*, **259**, 232.
 Bruner, E. C., Jr., and Rense, W. A. 1969, *Ap. J.*, **157**, 417.
 Clarke, J. T., Bowyer, S., Fahr, H. J., and Lay, G. 1984, *Astr. Ap.*, **139**, 389.
 Cowie, L. L., and Songaila, A. 1986, *Ann. Rev. Astr. Ap.*, **24**, in press.
 Crutcher, R. M. 1982, *Ap. J.*, **254**, 82.
 Dalaudier, F., Bertaux, J. L., Kurt, V. C., and Mironova, E. N. 1984, *Astr. Ap.*, **134**, 171.
 de Boer, K. S., Lenhart, H., van der Hucht, K. A., Kamperman, T. M., Kondo, Y., and Bruhweiler, F. C. 1986, *Astr. Ap.*, **157**, 119.
 Dupree, A. K., Baliunas, S. L., and Shipman, H. L. 1977, *Ap. J.*, **218**, 361.
 Evans, N. R., and Imhoff, C. 1985, *IUE Newsletter*, No. 28, p. 77.
 Fahr, H. J., Nass, H. U., and Rucinski D. 1985, *Astr. Ap.*, **142**, 476.
 Ferlet, R., Lallement, R., and Vidal-Madjar, A. 1986, *Astr. Ap.*, **163**, 204.
 Heintz, W. D. 1975, *Ap. J.*, **195**, 411.
 Joseph, C. L. 1985, Ph.D. thesis, University of Colorado.
 Lallement, R., Vidal-Madjar, A., and Ferlet, R. 1986, *Astr. Ap.*, in press.
 Lampton, M., Margon, B., and Bowyer, S. 1976, *Ap. J.*, **208**, 177.
 Landsman, W. B. 1984, Ph.D. thesis, Johns Hopkins University.
 Landsman, W. B., Henry, R. C., Moos, H. W., and Linsky, J. L. 1984, *Ap. J.*, **285**, 801.
 Landsman, W. B., Murthy, J., Henry, R. C., Moos, H. W., Linsky, J. L., and Russell, J. L. 1986, *Ap. J.*, **303**, 791.
 McClintock, W., Henry, R. C., Linsky, J. L., and Moos, H. W. 1978, *Ap. J.*, **225**, 465.
 McKee, C. F., and Ostriker, J. P. 1977, *Ap. J.*, **218**, 148.
 Strickland, D. S. 1980, *IUE Observatory Memo*.
 Struve, O., and Kilby, R. 1953, *Ap. J.*, **117**, 272.
 Turnrose, B. E., Thompson, R. W., Stone, D. F., and Perry, P. M. 1984, in *International Ultraviolet Explorer Image Processing Information Manual, Version 2.0 (CSC/TM-84/6058)*, pp. 6–19.
 Vidal-Madjar, A., Ferlet, R., Gray, C., and Lallement, R. 1986, *Astr. Ap.*, **155**, 407.
 Vidal-Madjar, A., and Gry, C. 1984, *Astr. Ap.*, **138**, 285.
 Vidal-Madjar, A., Laurent, C., Bruston, P., and Audouze, J. 1978, *Ap. J.*, **223**, 589.
 Weller, C. S., and Meier, R. R. 1981, *Ap. J.*, **246**, 386.

CECILLE GRY: ESA Satellite and Tracking Station, Apartado 54065, Madrid 28080, Spain

RICHARD C. HENRY, H. WARREN MOOS, and JAYANT MURTHY: Department of Physics and Astronomy, Johns Hopkins University, Baltimore, MD 21218

WAYNE B. LANDSMAN: S.A.S.C. Technologies, NASA Goddard Space Flight Center, Code 681, Greenbelt, MD 20771

JEFFREY L. LINSKY: Joint Institute For Laboratory Astrophysics, University of Colorado, Boulder, CO 80309

ALFRED VIDAL-MADJAR: Institut d'Astrophysique de Paris, 98bis Bd Arago, 75014 Paris, France